Evaluation of Gas-Solids Mixing Chamber through Cross Correlation and Hurst's Analysis

C. L. Briens, C. Mirgain, and M. A. Bergougnou
Chemical and Biochemical Engineering Dept., University of Western Ontario, Ont. N6A 5B9, Canada

M. Del Pozo and R. Loutaty
Total Raffinage Distribution, CERT, 76 700 Harfleur, France

Fast circulating fluidized-bed reactors are used for many applications, both in riser and downer modes. Typical residence times are in the order of a few hundreds of milliseconds. A good understanding of initial gas-solids contact must be reached to realize the full potential of such reactors. Effective and stable gas-solids mixing chambers were identified from the signals of simple and robust probes, which could be used in industrial and pilot plants. Criteria based on cross correlation or Hurst analysis provided consistent results. Although this study used simplified momentum probes, the criteria it developed can be applied to the signal of any fast-response sensor which is affected by local hydrodynamics. Temperature, capacitance, ultrasonic, or γ-ray absorption measurements could be used. Gas or liquid-liquid mixing chambers could also be optimized with the same criteria.

Introduction

Circulating fluidized beds have been widely used for industrial processes involving gas and solids. As shown by Bassi et al. (1993), their application to fast and complex reactions requires rapid and effective contact between gas and particles. Typical gas and particle residence times are of the order of a few hundreds of milliseconds. A good understanding of the gas-solids contact in the early stages of the reactions must be reached to realize full potential advantages of such reactors.

Two major configurations have been proposed. When gas and solids flow co-currently upward, the reactor is called a riser. A downer is a reactor where gas and solids flow co-currently downward. Extensive literature has shown the potential of downers over risers for fast reactions (Bai et al., 1990; Gross and Ramage, 1983; Murphy, 1992). Backmixing of solids in risers prevents high selectivity, whereas near plug-flow conditions in downers should allow higher selectivity. The stable, near plug-flow hydrodynamics of downer reactors requires a uniform dispersion of the solids into the gas phase in a mixing chamber, upstream of the downer. The complex mixing chamber hydrodynamics mean that experimental testing of many chamber geometries is needed to identify the best configurations. Since scale-up criteria are not well-known, measurements in pilot and industrial plants will be required.

A mixing chamber must meet two requirements. First, it must ensure good initial contact between gas and particles. Second, it must provide a uniform dispersion at the inlet of the downer. Recently, an "ammonia adsorption technique" was developed to characterize the initial contact between gas and particles in a mixing chamber (Mirgain et al., 1995). It is based on fast irreversible adsorption of ammonia on catalyst particles and provides direct and reliable results. This article investigates methods which test for the second requirement, a uniform dispersion at the exit of the mixing chamber.

Various experimental techniques have been proposed for instantaneous and local measurements of solids dispersions. Capacitance probes measure either cross-sectional average or local solids concentration (Irons and Chang, 1983; Soong et al., 1995; Williams et al., 1991), fiber optic probes measure either solids velocity or concentration (Dyakowski and Williams, 1993; Herbert et al., 1994; Li et al., 1991; Reh and Li, 1990; Sobocinski et al., 1995) and the Laser-Doppler technique measures solids and/or gas velocities (Hamdullahpur, 1985; Werther et al., 1991; Yang et al., 1993). None of these techniques can, however, be applied to pilot and industrial plants.

Momentum probes, which measure the two-phase momentum, are sturdier (Azzi et al., 1990; Bai et al., 1995; Yang et al., 1993). They unfortunately suffer from two limitations. First, they measure only the average momentum of the gas-

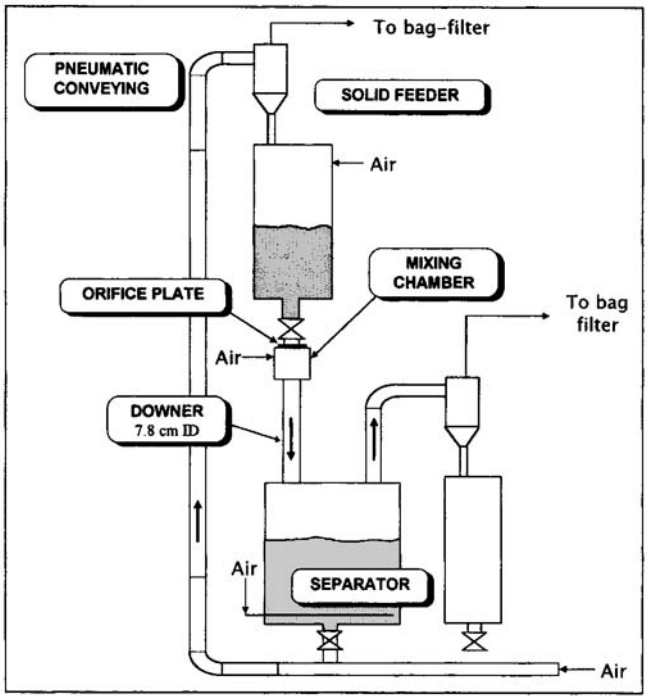

Figure 1. Experimental setup.

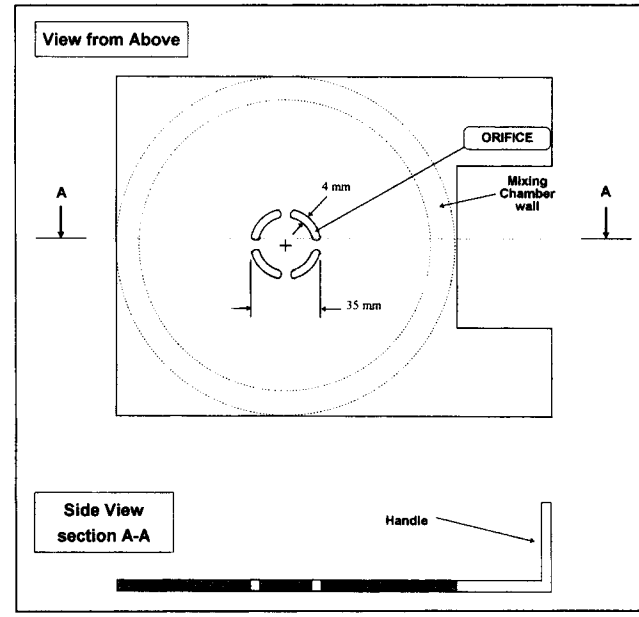

Figure 2. Solids feeder annular orifice plate.

solids mixture. When both phases have similar momenta, they cannot discriminate between gas and solids. Second, when the local flow direction is unknown, as in mixing chambers, they must be rotated until the flow direction is identified. This makes them unsuitable for industrial applications. Moreover, the flow direction will usually fluctuate rapidly and the average momentum cannot be measured.

The objective of this article is to present methods to characterize mixing chambers from the signals of simple and robust probes which could be used in industrial and pilot plants. Although these methods are demonstrated with signals from a simplified momentum probe, they could be applied to other measurements such as temperature or γ-ray absorption.

Experimental Setup

Figure 1 shows the experimental setup. Solid particles flow down from the feeder through an orifice plate to the 10-cm-dia., 30-cm-long, mixing chamber and the 7.8-cm-diameter downer which were made of stainless steel. Particles are removed from the gas by an inertial separator, a cyclone and a bag filter. After the experiment solids are returned to the feeder through a pneumatic return line. The solids were equilibrium Fluid-catalytic cracking (FCC) particles taken from an industrial fluid cracker. Their Sauter-mean diameter was about 70 μm, and their apparent density was 1,600 kg/m^3. The gas was air at room temperature with a 13% relative humidity.

A pressurized feeder delivers an annular solids jet to the mixing chamber. The solids are forced through four 4 mm wide slots as shown in Figure 2. Since the total solids residence time in the mixing chamber is of the order to 100 ms, fluctuations of the solids flow rate should be kept minimal. Delivering a constant mass flow of pressurizing air to the top of the feeder with a sonic nozzle results in stable solids flow. The time-averaged solids flow rate is determined by fluidizing the solids collected in the separator and measuring their mass. In all experiments reported in this article, the solids flow rate was maintained at about 400 g/s. Average fluctuations of the solids flow, as estimated from the fluctuations of the pressure drop through the orifice, were moderate (less than 5%) on a 1-ms time scale.

The mixing chamber is equipped with 8 jet nozzles supplied with constant air mass-flow rates from 8 calibrated sonic nozzles. The main advantage of sonic nozzles is that the mass-flow rate of air for a correctly selected upstream pressure is independent of the fluctuations in the downstream mixing chamber (Churchill, 1983). The total gas flow rate was 32 g/s, giving a jet velocity of 105 m/s and a superficial velocity of 5.8 m/s in the downer.

The eight jet nozzles through which the gas enters the mixing chamber can be oriented independently. For example, Figure 3a shows how the nozzles can be angled in the horizontal plane to induce a swirl. In some cases, only nozzles 1, 3, 5 and 7 were angled. Figure 3b shows how the nozzles could be inclined to hit the solids jet near its top, as in configuration A1, or near the bottom of the mixing chamber, as in configuration A2. Half the nozzles could also hit the solids jet near the top and the other half oriented to hit the solids jet near the bottom of the mixing chamber, as in configuration A3. Each one of configurations A1, A2 and A3 (Figure 3b) was tested in three different ways with all the nozzles straight, with all the nozzles angled to provide a swirl and with only half the nozzles angled (Figure 3a).

A new probe has been designed (Figure 4a). It did not provide specific information such as momentum, gas velocity or solid concentration. Its purpose, instead, was to provide a signal which represented the local, instantaneous mixing chamber hydrodynamics. Two major modifications have been made to the conventional momentum probe design. First, a stainless steel mesh at the probe tips eliminates the need for

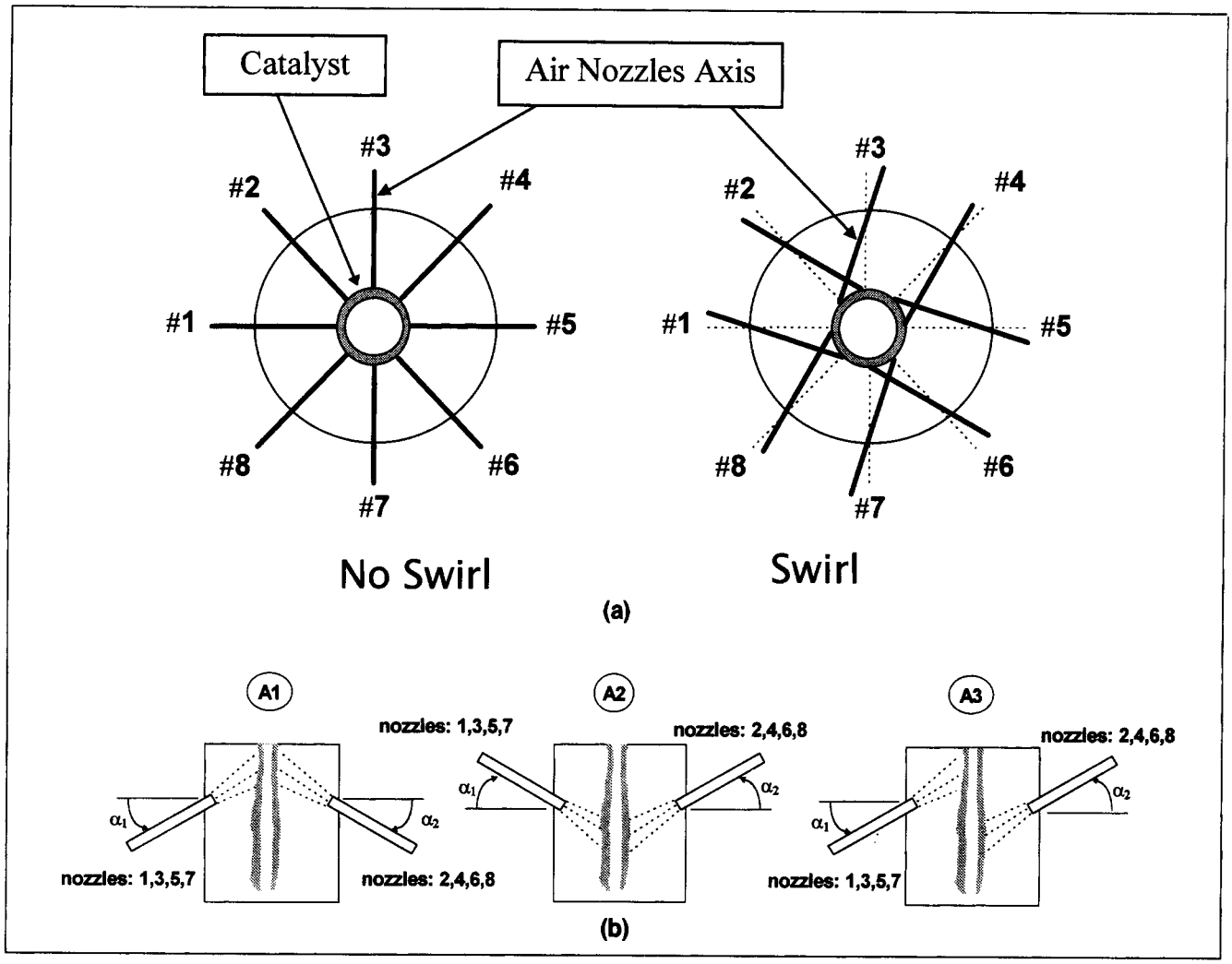

Figure 3. Orientations of eight gas nozzles.

(a) In the horizontal plane; (b) in the vertical plane.

back-flushing (Figure 4b). This simplifies operation, minimizes perturbations of the local hydrodynamics and prevents contamination of the instantaneous probe signal by fluctuations in back-flushing gas supply. Secondly, several upward probe tips are used simultaneously (Figure 4a). The seven probe tips are equally spaced in the downer cross-section and are located 6 cm downstream of the mixing chamber. Small diameter brass and PVC tubing (1.6 mm ID) connect the upward probe tips to the high-pressure port of differential fast response pressure transducers. The low pressure port of all the pressure transducers is connected to the same downward tip. The seven pressure signals were simultaneously recorded at a frequency of 1,000 Hz for about 30 s, using a 12-bit, 16-channel PC-LPM16 A/D card from National Instruments. The relatively large number of points (30,000 for each pressure) was required for accurate signal analysis. Power spectrum analysis of the pressure measurement system including mesh, tubing and transducers showed that frequencies up to 300 Hz could be detected, which is better than required for this study. Spectrum analysis indicated when the probe mesh filters needed cleaning, typically after 2–3 h of continuous operation.

Results and Discussion

The objective of the data analysis is to characterize the two-phase solids-gas dispersion produced by the mixing chamber. For a good quality gas-solid dispersion, a single hydrodynamic structure must extend over the whole downer cross-section. For example, if the solids jet flowing from the feeder was not broken up in the mixing chamber, parts of the downer cross-section would be occupied by a dense solids jet and gas would flow through the rest. The two independent methods which were developed to assess the dispersion quality tested whether the gas-solid dispersion displayed the same hydrodynamic characteristics at all seven probe locations. The first method used cross-correlation between the various probes: signals from probes which are within the same hydrodynamic structure vary together and are well cross correlated. The second used Hurst's analysis to characterize each probe signal; signals from probes which are within the same hydrodynamic structure are similar and exhibit the same Hurst characteristics.

Each method provided a measurement of the gas-solids dispersion quality. The first step averaged these measure-

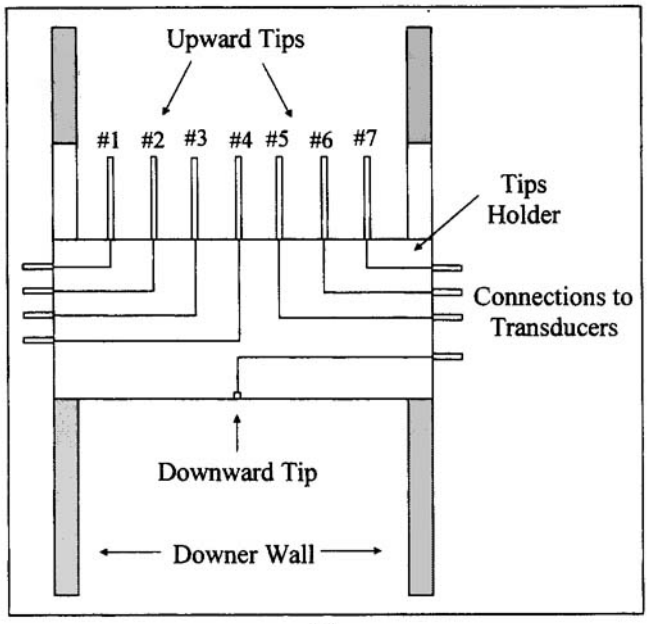

(a)

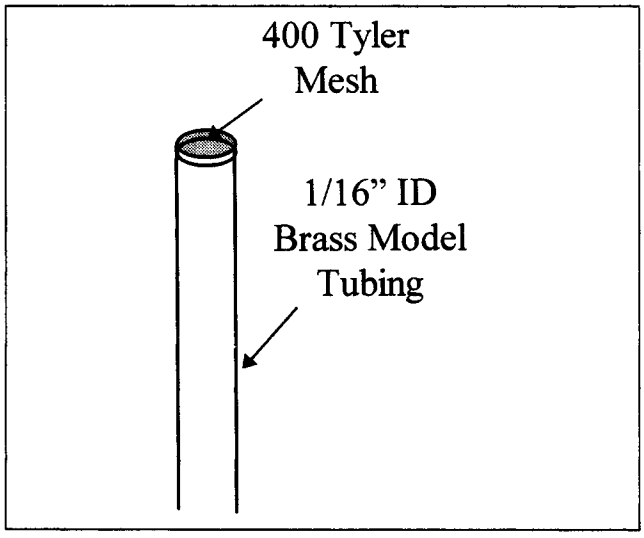

(b)

Figure 4. Probes used in this study.
(a) General side view; (b) detail of a probe tip.

ments over 30 s to estimate the time-averaged quality of the dispersion provided by each mixing chamber configuration. A good configuration should also continuously deliver a high dispersion quality. The second step was therefore to evaluate the stability of the dispersion quality on a time scale of 100 ms, which corresponds to the average gas residence time in the chamber. Finally, in the third step, the most promising mixing chamber configurations were identified.

Figure 5 shows an example of a raw probe signal over 10% of the measurement time. Similar signals were obtained from other probes. The signals fluctuated at a high frequency but did not display regular periodicity.

Figure 6 shows a signal from the same probe over the whole measurement time. For this figure only, the signal was

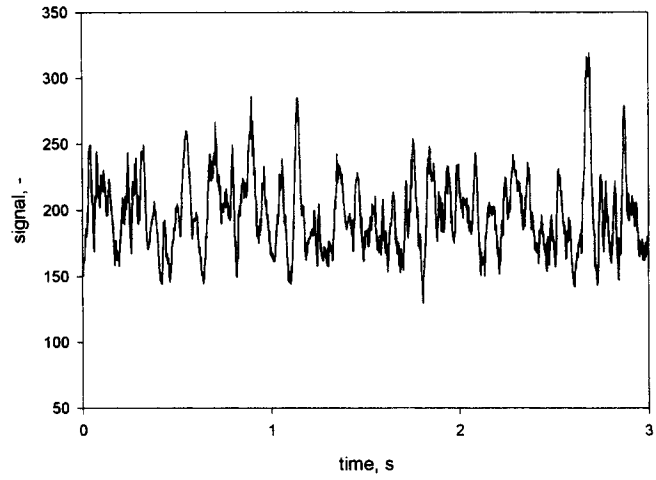

Figure 5. Example of raw probe signal (probe No. 1 of Figure 4a).

smoothed to eliminate high frequency fluctuations. The signals from the eight probes drifted together.

Figure 7 gives an example of the time-average of the signals delivered by each probe. As shown earlier in the introduction, such figures provide useful information but cannot reliably identify the best mixing chambers.

Time-averaged quality of dispersion

The two independent methods tested whether the gas-solid dispersion displayed the same hydrodynamic characteristics at all seven probe locations. The first method used cross-correlation, while the second used Hurst's analysis.

Methods Based on Cross-Correlation. An earlier article (Mirgain et al., 1997) presented a cross-correlation analysis which is limited to mixing chambers where the solids are fed through a circular orifice. This article presents a more general and complete analysis.

If two probes are within the same hydrodynamic structure, their signals will vary together. The cross-correlation obtained from the two probe signals should, thus, be near 1.

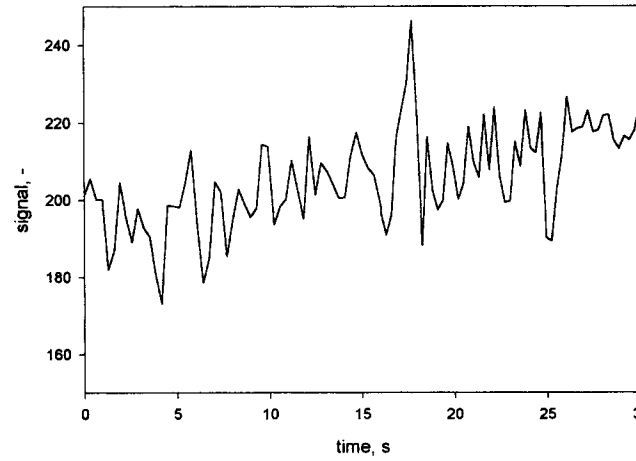

Figure 6. Example of smoothed probe signal (using the Lowess algorithm) (probe No. 1 of Figure 4a).

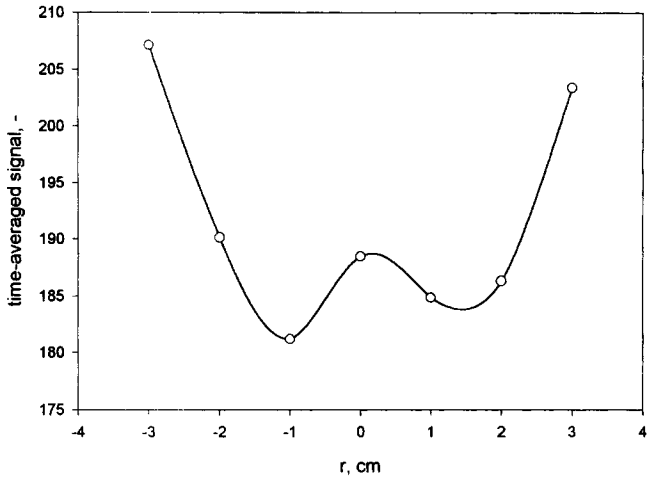

Figure 7. Example of radial profile obtained with time-averaged probe signals.

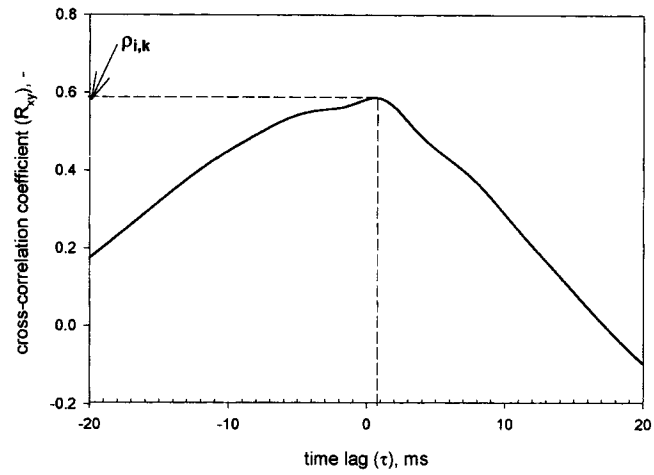

Figure 8. Example of the variation of the cross-correlation coefficient with the time lag for a given chunk.

Cross correlation is between the probe at $r = 0$ and the probe at $r = -3$ cm.

Considering the signal $x(t)$ delivered by a probe and the signal $y(t)$ delivered by another probe, their normalized cross-correlation coefficient for a time lag τ is given by

$$R_{xy}(\tau) = \frac{1}{t_2 - t_1} \int_{t_1}^{t_2} \left(\frac{x(t) - x_m}{\sigma_x} \right) \left(\frac{y(t+\tau) - y_m}{\sigma_y} \right) dt \quad (1)$$

where x_m and σ_x are, respectively, the average and standard deviation of $x(t)$ over the interval $[t_1, t_2]$ and y_m and σ_y are the average and standard deviation of $y(t)$ over the interval $[t_1 + \tau, t_2 + \tau]$. As shown by Figure 6, the probe signals drifted slowly over time. If $R_{xy}(\tau)$ had been calculated over a time interval $[t_1, t_2]$ equal to the 30 s measurement time, the signal drift would have caused erroneous results. To minimize the effect of the drift, each signal was divided in N_c chunks of length $(t_2 - t_1) = \Delta t_c$. For each chunk, the averages x_m and y_m, the standard deviations σ_x and σ_y, and the cross-correlation coefficient $R_{xy}(\tau)$ were calculated.

Figure 8 shows an example for such a chunk of the cross-correlation coefficient between the central probe and the probe nearest the chamber wall. The chunk length was 100 ms, which corresponds to the average gas residence time in the chamber. The maximum correlation coefficient was obtained for a time lag τ of about 1 ms. The maximum value $\rho_{i,k}$ of R_{xy} was thus determined for each chunk i and probe combination k. There were 7 probes and, therefore, 21 possible binary combinations of probe signals $x(t)$ and $y(t)$.

The "chunk correlation coefficient" $\bar{\rho}_i$ was calculated for each chunk i by averaging for all the probe combinations

$$\bar{\rho}_i = \frac{1}{21} \sum_{k=1}^{21} \rho_{i,k} \quad (2)$$

Similarly, the chunk coefficient of variation was obtained from

$$C_{v,i} = \frac{\sqrt{\frac{1}{21} \sum_{k=1}^{21} (\rho_{i,k} - \bar{\rho}_i)^2}}{\bar{\rho}_i} \quad (3)$$

If all probes are in the same hydrodynamic structure, they should be well correlated and a high value, near 100%, should be obtained for the following time-averaged mixing index

$$\mathrm{MI} = \frac{100}{N_c} \sum_{i=1}^{N_c} \bar{\rho}_i \quad (4)$$

If the gas-solid dispersion is uniform, all 21 probe combinations should give about the same correlation coefficient $\bar{\rho}_i$ and the chunk variation coefficients $C_{v,i}$ should be small. The following time-averaged uniformity index should, thus, be near 100%

$$\mathrm{UI} = 100 \left[1 - \frac{1}{N_c} \sum_{i=1}^{N_c} C_{v,i} \right] \quad (5)$$

Figures 9a and 9b show the effect of the chunk length Δt_c on the mixing index MI and the uniformity index UI. Although both indices were affected by the chunk length, the relative ranking of the 59 tested mixing chamber geometries was not greatly affected.

Methods Based on Hurst's Analysis. If the gas-solid dispersion is uniform, all probes yield signals which have the same structure. The structure of a time series may be characterized by its fractal dimension. Several authors have used the fractal dimension of pressure or momentum probe signals to characterize the hydrodynamics of circulating fluidized-bed risers. van der Stappen et al. (1993) found that the fractal dimension of pressure measurements varied between the wall and the center of the riser, and between its bottom and top. Bouillard and Miller (1996) found that the fractal dimension of pressure fluctuations in a riser was low. Bai et al. (1996) found that the fractal dimension of a momentum probe signal varied between the wall and the center regions of a riser. They attributed this difference to a core-annulus structure which imposes different hydrodynamics in the wall and center regions. While the fractal dimension is a powerful tool, it

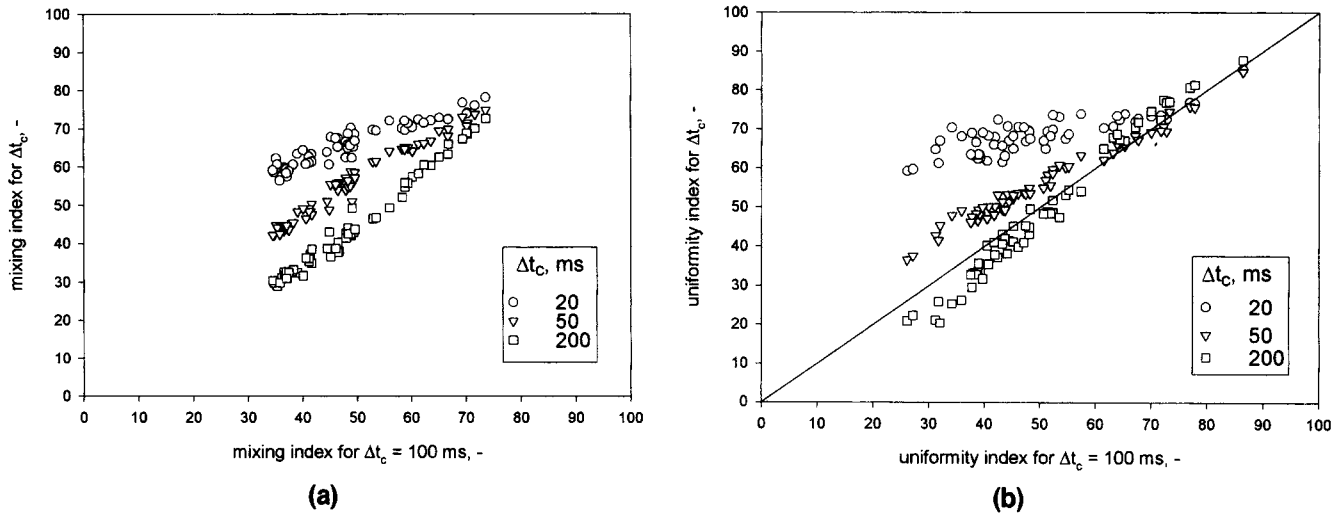

Figure 9. Effect of chunk length on the time-averaged indices based on cross-correlation analysis for the 59 tested mixing chamber configurations.

(a) Mixing index; (b) uniformity index.

suffers from two main drawbacks: its sensitivity to noise and its long computation time.

Hurst's (1951) analysis is a quicker, simpler and more robust alternative to fractal analysis. It quantifies both the persistence and the cycle time of a time series. For a random walk process such as Brownian motion, there is no correlation between past and future increments and the Hurst exponent is 0.5. An exponent greater than 0.5 indicates persistence in the data, that is, the trend in the time series, whether increasing or decreasing, will likely continue. An exponent less than 0.5 indicates antipersistence in the data, that is, the trend will likely reverse itself. If all the probes belong to the same hydrodynamic structure, their signal will exhibit the same persistence, that is, the same Hurst exponent.

The V statistic was proposed by Hurst (1951) to find the cycle length of a nonperiodic system. It is defined from the rescaled range $(R/S)_{\tau_H}$ at a subperiod length τ_H

$$V_{\tau_H} = \frac{(R/S)_{\tau_H}}{\sqrt{\tau_H}} \tag{6}$$

A cyclic system will exhibit a clear maximum of the V statistic for a value of τ_H which corresponds to its cycle time. If all the probes belong to the same hydrodynamic structure, their signal will exhibit the same cyclic time.

Briens et al. (1997) used Hurst's analysis to identify flow regime transitions and gas maldistribution in gas-liquid-solid fluidized beds. This article uses the same analysis to characterize the gas-solid dispersion at the exit of the mixing chamber. The basic calculation procedures are provided elsewhere (Briens et al., 1997).

Figure 10 shows how Hurst's analysis was applied to a probe signal. The rescaled range (R/S) was first plotted against the subperiod length τ_H in log-log coordinates (Figure 10a). The Hurst exponents shown in Figure 10b were obtained from Figure 10a by applying a smoothing spline to the curve and taking its derivative. Two regions which are connected by a smooth transition region appear at both ends of the subperiod length scale (these two regions were also found by Briens et al. (1997) in gas-liquid-solid fluidized beds). All mixing chamber configurations gave similar results. The "high frequency Hurst exponent" $H_{\max}$ is obtained for subperiod lengths of 20 to 60 ms, that is, for frequencies of 15 to 50 Hz. The "low frequency Hurst exponent" $H_{\min}$ is obtained for subperiod lengths of 1,000 to 3,000 ms, that is, for frequencies of 0.15 to 0.5 Hz. The high frequency Hurst exponent was always larger than 0.5, indicating a persistent system behavior, that is, the trend will likely propagate itself. The low frequency Hurst exponent was always smaller than 0.5, indicating an antipersistent system behavior, that is, the trend will likely reverse itself.

Figure 10c shows that the V statistic of a typical probe signal displayed a clear maximum. The subperiod length τ_v at which this maximum occurred is the system cycle length. Interestingly, it is near the 100 ms mean residence time of the gas in the mixing chamber. The maximum value $V_{\max}$ of the V statistic measures the strength of the cyclic, nonperiodic behavior of the probe signal.

A similar analysis of the solids feed rate fluctuations established that they did not cause the fluctuations measured by the probes at the exit of the mixing chamber. The instantaneous solids feed rate was obtained from the instantaneous pressure drop through the orifice of the solids feeder. Hurst's analysis showed that the solids feed rate fluctuations were antipersistent at low subperiod lengths. This is the exact opposite to what was observed for probe signals (Figure 10). The antipersistent behavior of the feeder at the small subperiods also indicates that it was operating properly: if there was a small increase in the instantaneous feed rate, it was immediately followed by a compensating decrease. Figure 11 shows that no cycle length could be found for the solids feed rate, in sharp contrast to what was found for the probe signal (Figure 10c).

If all probes belong to the same hydrodynamic structure, they should have the same low and high frequency Hurst exponents $H_{\min}$ and $H_{\max}$, the same cycle length τ_v, and the same maximum value $V_{\max}$ of the V statistic. One can, thus,

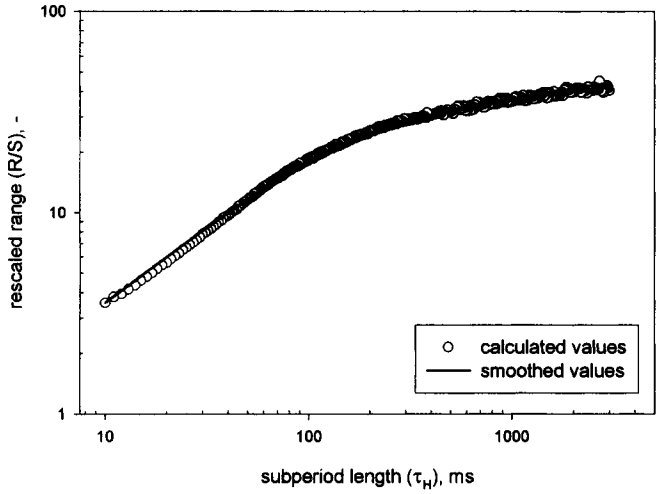

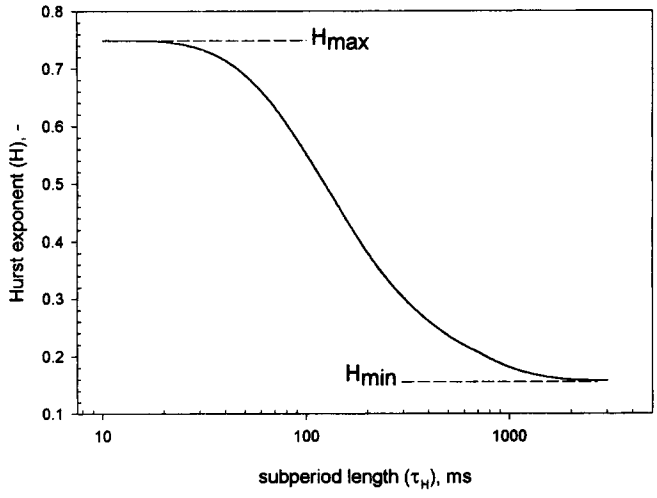

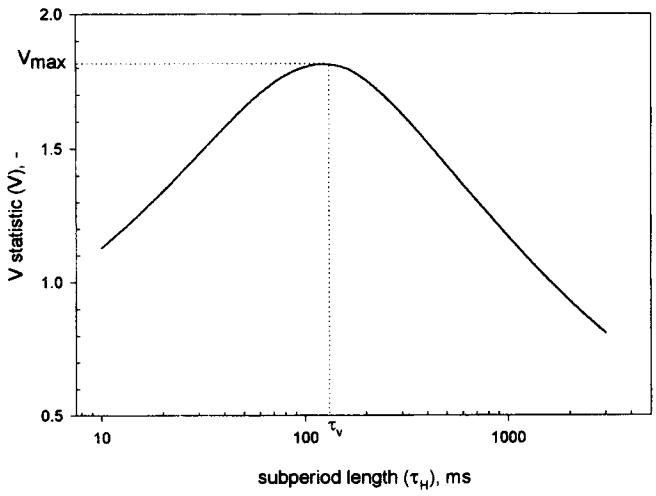

Figure 10. Hurst's analysis of a typical probe signal.
(a) Rescaled range; (b) Hurst exponent; (c) V statistic.

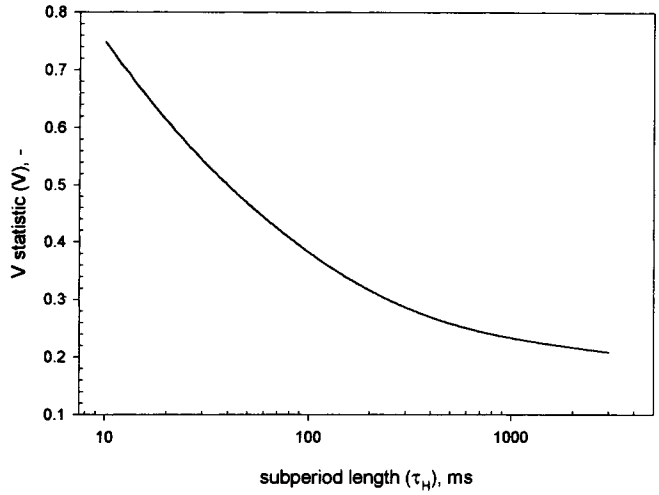

Figure 11. Hurst's analysis of the feeder orifice plate fluctuations: *V* statistic.

define four indices which are calculated from a coefficient of variation and which will be high if the probes are within the same hydrodynamic structure and low otherwise

$$I_{H_{max}} = 100\left[1 - \frac{\sqrt{\frac{1}{7}\sum_{j=1}^{7}\left(H_{max,j} - \frac{1}{7}\sum_{j=1}^{7} H_{max,j}\right)^2}}{\frac{1}{7}\sum_{j=1}^{7} H_{max,j}}\right] \quad (7)$$

$$I_{H_{min}} = 100\left[1 - \frac{\sqrt{\frac{1}{7}\sum_{j=1}^{7}\left(H_{min,j} - \frac{1}{7}\sum_{j=1}^{7} H_{min,j}\right)^2}}{\frac{1}{7}\sum_{j=1}^{7} H_{min,j}}\right] \quad (8)$$

$$I_{\tau V} = 100\left[1 - \frac{\sqrt{\frac{1}{7}\sum_{j=1}^{7}\left(\tau_{v,j} - \frac{1}{7}\sum_{j=1}^{7} \tau_{v,j}\right)^2}}{\frac{1}{7}\sum_{j=1}^{7} \tau_{v,j}}\right] \quad (9)$$

$$I_{V_{max}} = 100\left[1 - \frac{\sqrt{\frac{1}{7}\sum_{j=1}^{7}\left(V_{max,j} - \frac{1}{7}\sum_{j=1}^{7} V_{max,j}\right)^2}}{\frac{1}{7}\sum_{j=1}^{7} V_{max,j}}\right] \quad (10)$$

Figure 12 compares the average of the two time-averaged indices based on cross-correlation analysis (MI and UI) to the average of the four indices based on Hurst's analysis (I_{Hmax}, I_{Hmin}, $I_{\tau V}$, I_{vmax}). The advantage of Hurst's analysis is that it

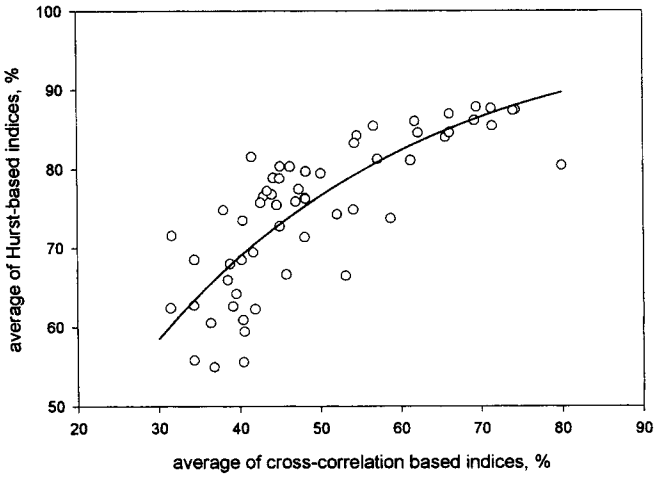

Figure 12. Average of four indices based on Hurst's analysis vs. average of two time-averaged indices based on cross-correlation analysis for the 59 tested mixing chamber configurations.

does not require simultaneous acquisition of the data from all the probes: the signal from each probe can be acquired separately or a single probe may be moved to different locations.

Stability of dispersion quality

A good mixing chamber should provide a gas-solid dispersion quality which is not only good on average, but will not fail even for short time intervals. The dispersion quality must be stable. Three different criteria were developed to evaluate the stability of the dispersion. The first, called "mixing stability" (MS), was obtained from the chunk correlation coefficients $\bar{\rho}_i$

$$\mathrm{MS} = 100\left[1 - \frac{\sqrt{\frac{1}{N_c}\sum_{i=1}^{N_c}(\bar{\rho}_i - 0.01\ \mathrm{MI})^2}}{0.01\ \mathrm{MI}}\right] \quad (11)$$

The second, called uniformity stability (US), was obtained from the chunk variation coefficients $C_{v,i}$

$$\mathrm{US} = 100\left[1 - \frac{\sqrt{\frac{1}{N_c}\sum_{i=1}^{N_c}((1-C_{v,i}) - 0.01\ \mathrm{UI})^2}}{0.01\ \mathrm{UI}}\right] \quad (12)$$

The third criterion was obtained by characterizing the structure of the time series of the chunk correlation coefficients $\bar{\rho}_i$ as a function of the average chunk time. Figure 13 shows an example of such a time series, which was obtained for a chunk length of 20 ms. Figure 13a shows that the chunk correlation coefficient fluctuated over a wide range. Figure 13b, which was obtained by smoothing out the high frequencies of the same time series, shows the chunk correlation coefficient drifted over the 30-s run length. Figure 14 presents the results of Hurst's analysis of the same time series. Figure 14a shows that there was a single Hurst exponent H and Figure 14b shows that there was no cycle time. This Hurst exponent provided the third stability criterion.

Figure 15 shows that the three stability criteria gave consistent results. The Hurst exponent and the mixing stability are well correlated (Figure 15a). The uniformity and mixing stabilities are also well correlated (Figure 15b). The spread of individual values about the regression line in both figures, however, indicates that the use of all three criteria is required to eliminate unstable mixing chambers.

Figures 16 and 17 demonstrate how crucial was the selection of the chunk length. There was no correlation between the mixing stability calculated for a chunk length of 100 ms

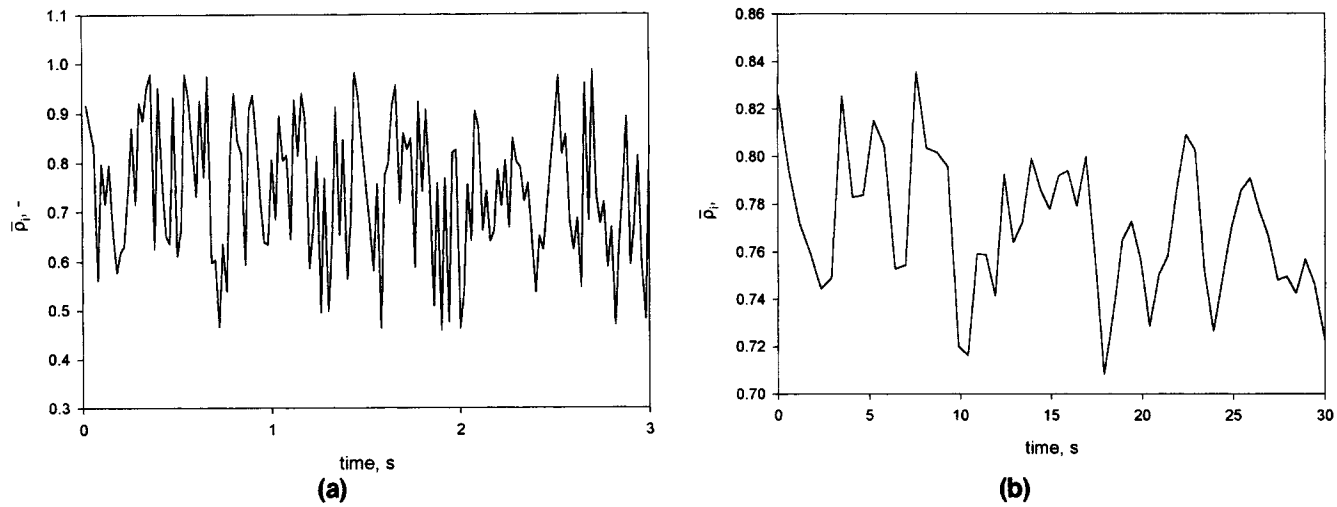

Figure 13. Example of the time series formed with the chunk correlation coefficient, using a chunk length $\Delta t_c = 20$ ms.

(a) Raw signal; (b) smoothed signal (using the Lowess algorithm).

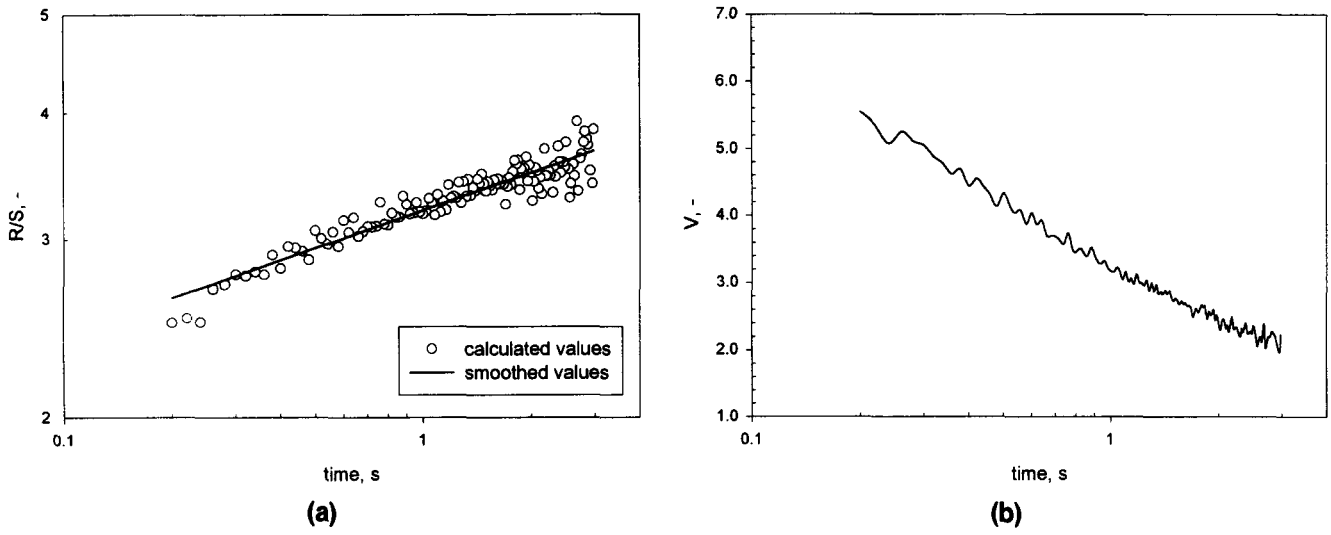

Figure 14. Hurst's analysis applied to the time series formed with the chunk correlation coefficient, using a chunk length $\Delta t_c = 20$ ms.

(a) Rescaled range; (b) V statistic.

and the mixing stabilities calculated for other chunk lengths (Figure 16). Similar results were obtained with the uniformity stability (Figure 17). This crucial effect of the chunk length is in sharp contrast with what was observed with the time-averaged indices (Figure 9). When evaluating a mixing chamber, it is therefore essential to clearly define the process requirements, that is, at what time scale is mixing required.

Figure 18 was obtained with a chunk length of 100 ms, which corresponds to the average gas residence time in the mixing chamber. The spread of individual values about the regression curve shows that both sets of criteria are needed to identify good mixing chambers. On the other hand, good correlation on this time scale between the calculated stabilities and time-averaged indices indicates that, in general, a mixing chamber which provides a good gas-solid dispersion will also provide a stable dispersion on a 100-ms time scale.

Figure 19 shows, however, that stability at the 20-ms level was inversely correlated with good mixing. Good mixing, as characterized by the average of the mixing and uniformity indices, was associated with a low Hurst exponent calculated with 20 ms long chunks. All the Hurst exponents were well below 0.5, indicating antipersistent behavior, that is, any increase in the chunk correlation coefficient is likely to be followed by a decrease in this coefficient. The best mixing chambers give Hurst exponents of about 0.11. An exponent of 0 would correspond to a perfectly random signal. The best mixing chambers thus combine a stable mixing quality on a time scale of the average residence time with nearly random

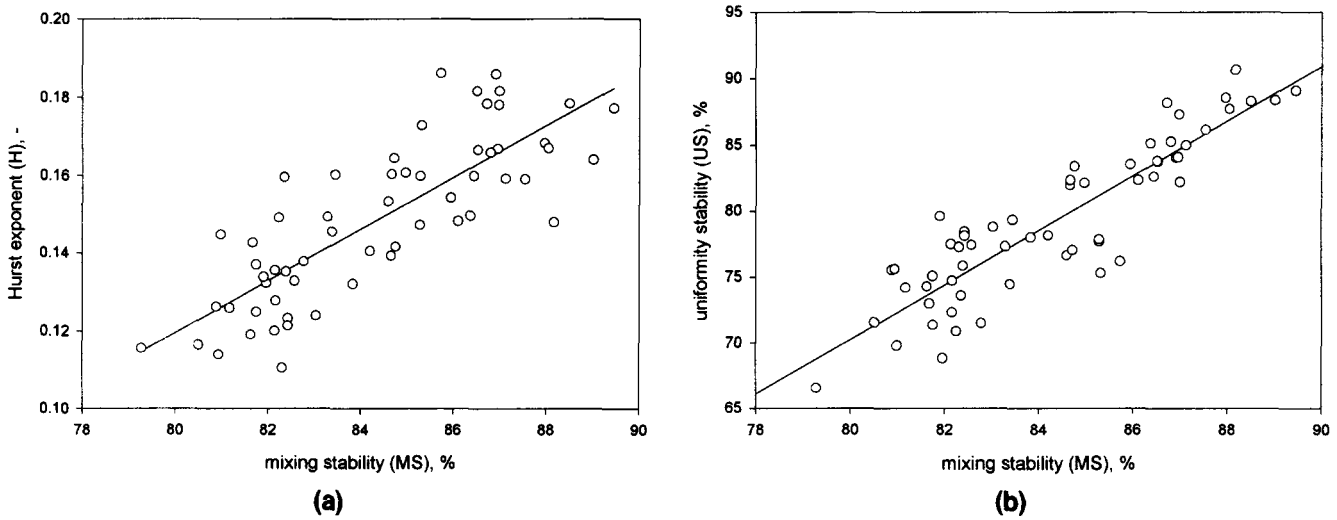

Figure 15. Three criteria used to characterize the stability of gas-solid dispersion using a chunk length $\Delta t_c = 20$ ms for the 59 tested mixing chamber configurations.

(a) Comparison of Hurst exponent and mixing stability; (b) comparison of uniformity stability and mixing stability.

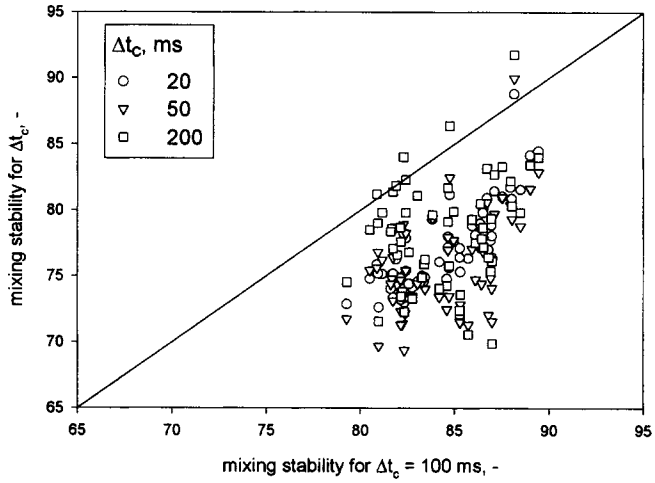

Figure 16. Effect of chunk length on mixing stability for 59 tested mixing chamber configurations.

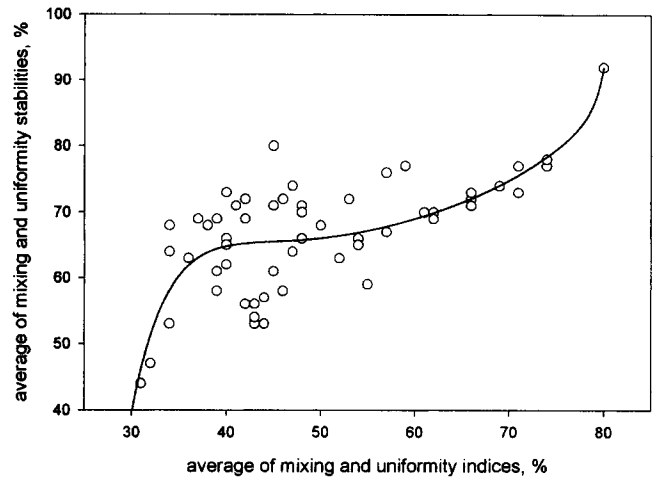

Figure 18. Relationship between stabilities, calculated with a chunk length of 100 ms, and time-averaged indices for the 59 tested mixing chamber configurations.

fluctuations of the mixing quality on a time scale of a few milliseconds.

Selection of best mixing chamber geometry

Table 1 shows the various indices and stabilities obtained with the top ten mixing chamber configurations. The chambers were ranked according to the average of the indices based on Hurst's analysis and the time-averaged indices based on the cross-correlation analysis.

Configuration No. 15 would, at first, appear to provide the best gas-solid dispersion. The Hurst exponent calculated with 20 ms chunks was, however, rather high for a good mixing chamber (Figure 19). The average exponent H_{max} obtained from the raw probe signals (Figure 10b) also appeared to be much smaller than for the other mixing chambers: the signals appeared slightly antipersistent while all the other configurations gave persistent signals. Subsequent tests indicated that this mixing chamber was poor: although all the probes were within the same hydrodynamics region, they were all in a dilute phase core and most of the solids were concentrated in a dense wall annulus. This demonstrates how important it is to extract all possible information from the probe signals.

Replicate experiments confirmed this ranking. Indices MI and UI varied by less than 1% and indices MS and US by less than 5% between replicate experiments.

Conclusions

Effective and stable gas-solids mixing chambers were identified from the signals of simple and robust probes. Criteria based on cross-correlation or Hurst analysis provided consistent results.

Although the present study used simplified momentum probes, it developed criteria which can be applied to the signal of any fast-response sensor which is affected by local hy-

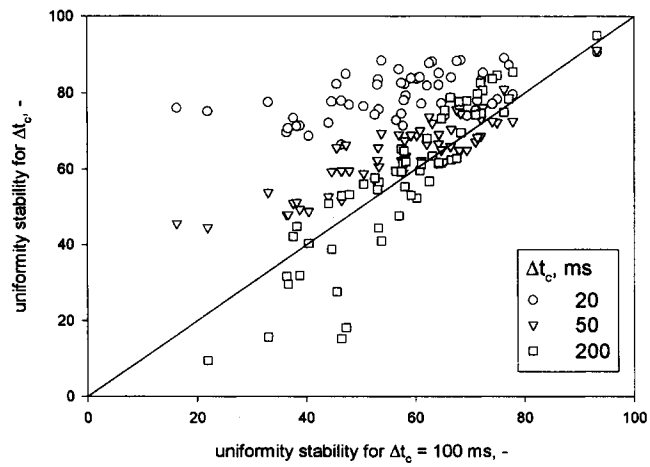

Figure 17. Effect of chunk length on uniformity stability for 59 tested mixing chamber configurations.

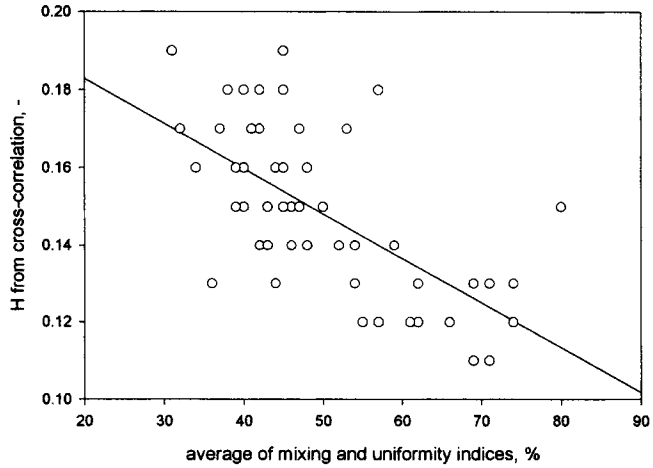

Figure 19. Relationship between the Hurst exponent calculated from 20 ms long chunks and the average of mixing and uniformity indices for 59 tested mixing chamber configurations.

Table 1. Results Obtained with Ten Best Mixing Chambers*

Config. No.	Avg. of All Indices	MI	UI	$I_{H\max}$	$I_{H\min}$	$I_{\tau V}$	$I_{V\max}$	MS	US	$H_{\max}$	H ($\Delta t_c = 20$ ms)
15	85	74	86	93	84	97	82	90	93	0.46	0.15
31	83	70	78	97	89	95	89	79	78	0.67	0.13
30	83	72	77	96	94	93	83	78	75	0.71	0.12
46	81	69	73	97	88	94	87	79	74	0.71	0.11
25	81	67	72	94	97	90	89	76	72	0.69	0.13
44	80	70	73	96	87	94	80	76	69	0.70	0.13
56	80	67	72	96	91	93	84	77	71	0.67	0.11
29	79	65	67	96	89	93	88	76	68	0.70	0.12
57	78	62	70	97	73	97	90	75	71	0.66	0.12
32	77	64	68	94	90	91	79	75	68	0.66	0.12
Max. for 59 configs.	85	74	86	97	97	98	93	90	93	0.75	0.19
Min. for 59 configs.	47	35	26	60	57	62	1	69	16	0.41	0.11

*In all cases with the exception of the last column, the chunk length is $\Delta t_c = 100$ ms.

drodynamics. Similar results could be obtained with temperature, capacitance, ultrasonics or γ-ray absorption measurements.

The methods presented in this article could also be applied to mixing chambers which involve other phases. For example, gas or liquid-liquid mixing chambers could thus be optimized.

Acknowledgments

The authors would like to thank Total Petroleum for its financial support. The authors gratefully acknowledge help with Hurst's analysis from Dr. J. Hay and L. Briens.

Literature Cited

Azzi, M., P. Turlier, J. F. Large, and J. R. Bernard, "Use of Momentum Probe and Gamma-Densitometry to Study Local Properties of Fast Fluidised Beds," *3rd Int. Conf. on Circulating Fluidized Beds (CFB3)*, Nagoya, Japan, p. 189 (Oct. 15–18, 1990).

Bai, D., E. Shibuya, Y. Masuda, N. Nakagawa, and K. Kato, "Flow Structure in a Fast Fluidized Bed," *Chem. Eng. Sci.*, **51**, 957 (1996).

Bai, D., E. Shibuya, Y. Masuda, K. Nishio, N. Nakagawa, and K. Kato, "Distinction between Upward and Downward Flows in Circulating Fluidized Beds," *Powder Technol.*, **84**, 75 (1995).

Bai, D., T. Jin, and N. Gan, "Radial Profiles of Local Solids Concentration and Velocity in a Concurrent Downflow Fast Fluidized Bed," *3rd Int. Conf. on Circulating Fluidized Beds (CFB3)*, Nagoya, Japan, pp. 157–162 (Oct 15–18, 1990).

Bassi, A. S., C. L. Briens, and M. A. Bergougnou, "Short Contact Time Fluidized Reactors (SCTFR'S)," *Circulating Fluidized Bed Technology IV (CFB4)*, p. 15, Somerset, PA (Aug. 1–5, 1993).

Bouillard, J. X., and A. L. Miller, "Experimental Investigations of Chaotic Hydrodynamic Attractors in Circulating Fluidized Beds," *Powder Technol.*, **79**, 211 (1994).

Briens, C. L., L. A. Briens, J. Hay, C. Hudson, and A. Margaritis, "Application of Hurst Analysis to the Detection of Minimum Fluidization and Gas Maldistribution in Gas-Liquid-Solid Fluidized Beds," in press *AIChE J.* (1997).

Churchill, S. W., "Compressible Flow," *Handbook of Fluids in Motion*, N. Cheremisinoff and S. Gupta, eds., Chapter 8, p. 211, Ann Arbor Science Publishers (1983).

Dyakowski, T., and R. A. Williams, "Measurement of Particle Velocity Distribution in a Vertical Channel," *Powder Technol.*, **77**, 135 (1993).

Gross, B., and M. P. Ramage, "FCC Reactor with a Downflow Reactor Riser," U.S. Patent 4385985 (1983).

Hamdullahpur, P., "Two-Phase Flow Behavior in the Freeboard of a Gas Fluidized Bed," PhD Thesis, Technical Univ. of Nova Scotia, Canada (1985).

Harris, B. J., J. F Davidson, and Y. Xue, "Axial and Radial Variation of Flow in Circulating Fluidized Bed Risers," *Circulating Fluidized Bed Technology IV (CFB4)*, Somerset, PA, p. 103 (Aug. 1–5, 1993).

Herbert, P. M., T. A. Gauthier, C. L. Briens, and M. A. Bergougnou, "Application of Fiber Optic Reflection Probes to the Measurement of Local Particle Velocity and Concentration in Gas-Solid Flow," *Powder Technol.*, **80**, 243 (1994).

Hurst, H. E., "Methods of Using Long-Term Storage in Reservoirs," *Trans. ASCE*, **116**, 770 (1951).

Irons, G. A., and G. S. Chang, "Dispersed Powder Flow through Vertical Pipes," *Powder Technol.*, **34**, 233 (1983).

Li, H., Y. Xia, Y. Tung, and M. Kwauk, "Micro-Visualization of Clusters in a Fast Fluidized Bed," *Powder Technol.*, **66**, 231 (1991).

Mirgain, C., C. L. Briens, and M. A. Bergougnou, "A New Technique for the Measurement of Fast Initial Gas-Solids Mixing in Short-Contact Time Reactors," *Fluidization and Fluid-Particle Systems*, Preprints, AIChE Meeting, Miami Beach, p. 152 (Nov. 12–17, 1995).

Mirgain, C., C. L. Briens, M. Del Pozo, R. Loutaty, and M. A. Bergougnou, "A New Technique for the Evaluation of a Circulating Fluidized Bed Mixing," *Powder Technol.*, in press (1997).

Murphy, J. R., "Evolutionary Design Changes Mark FCC Process," *Oil and Gas J.*, 49 (May 18, 1992).

Reh, L., and J. Li, "Measurement of Voidage in Fluidized Beds by Optical Probes," *Int. Conf. on Circulating Fluidized Beds (CFB3)*, Nagoya, Japan, p. 163 (Oct. 15–18, 1990).

Sobocinski, D. A., B. J. Young, and H. I. de Lasa, "New Fiber-Optic Method for Measuring Velocities of Strands and Solids Hold-Up in Gas-Solids Downflow Reactors," *Powder Technol.*, **83**, 1 (1995).

Soong, C. H., K. Tuzla, and J. C. Chen, "Experimental Determination of Cluster Size and Velocity in Circulating Fluidized Bed," *Fluidization VIII*, Preprints, Tours, France, pp. 457–465 (May 14–19, 1995).

van der Stappen, M. L. M., J. C. Schouten, and Cor M. van den Bleek, "Application of Deterministic Chaos Analysis to Pressure Fluctuation Measurements in a 0.96 m^2 CFB Riser," *Circulating Fluidized Bed Technol. IV (CFB4)*, Somerset, PA, pp. 54–61 (Aug. 1–5, 1993).

Werther, J., E. U. Hartge, and D. Rensner, "Measuring Techniques for Gas-Solids Fluidized Bed Reactors," in *La Fluidisation*, Récents progrès en Génie Chimique, C. Laguerie and P. Guigon, eds., **5** (11), Lavoisier Technique et Documentation (1991).

Williams, R. A., C. G. Xie, F. J. Dickin, S. J. R. Simons, and M. S. Beck, "Review: Multi-phase Flow Measurements in Powder Processing," *Powder Technol.*, **66**, 203 (1991).

Yang, Y. L., J. Jin, J. Q. Yu, J. X. Zhu, and H. T. Bi, "Local Slip Behaviours in the Circulating Fluidized Bed," *AIChE Symposium Series*, **89** (296), 81 (1993).

Manuscript received July 9, 1996, and revision received Jan. 23, 1997.